
Article:
Rap, A, Scott, CE, Reddington, CL et al. (2018) Enhanced global primary production by biogenic aerosol via diffuse radiation fertilization. Nature Geoscience, 11 (9). pp. 640-644. ISSN: 1752-0894

https://doi.org/10.1038/s41561-018-0208-3

Enhanced global primary production by biogenic aerosol via diffuse radiation fertilization

A. Rap[1*], C.E. Scott[1], C.L. Reddington[1], L. Mercado[2,3], R.J. Ellis[3], S. Garraway[4], M.J. Evans[4], D.J. Beerling[5], A.R. MacKenzie[6], C.N. Hewitt[7], D.V. Spracklen[1]

[1] School of Earth and Environment, University of Leeds, Leeds, UK

[2] College of Life and Environmental Sciences, Geography Department, University of Exeter, Exeter, UK

[3] Centre for Ecology and Hydrology, Wallingford, UK

[4] Department of Chemistry, University of York, York, UK

[5] Department of Animal and Plant Sciences, University of Sheffield, Sheffield, UK

[6] Birmingham Institute of Forest Research (BIFoR), University of Birmingham, Birmingham, UK

[7] Lancaster Environment Centre, Lancaster University, Lancaster, UK

[*] Corresponding author. Email: a.rap@leeds.ac.uk

Terrestrial vegetation releases large quantities of plant volatiles into the atmosphere that can then oxidise to form secondary organic aerosol. These particles affect plant productivity via the diffuse radiation fertilisation effect through altering the balance between direct and diffuse radiation reaching the Earth's surface. Here, using a suite of models describing relevant coupled components of the Earth system, we quantify the impacts of biogenic secondary organic aerosol on plant photosynthesis via this fertilisation effect. We show that this leads to a net primary productivity enhancement of 1.23 Pg C a^{-1} (range 0.76-1.61 Pg C a^{-1} due to uncertainty in biogenic secondary organic aerosol formation). Notably, this productivity enhancement is twice the mass of biogenic volatile organic compound emissions (and ~30 times larger than the mass of carbon in biogenic secondary organic aerosol) causing it. Hence, our simulations indicate that there is a strong positive ecosystem feedback between biogenic volatile organic compound emissions and plant productivity via plant-canopy light-use efficiency. We estimate a gain of 1.07 in global biogenic volatile organic compound emissions resulting from this feedback.

Biogenic volatile organic compounds (BVOCs) such as isoprene and monoterpenes, produced by plants in large quantities[1], play an important role in biosphere-atmosphere-climate interactions and feedbacks[2,3]. While controlled by physiological processes, and modulated by biotic stresses such as herbivory, the emission rates of BVOCs also respond promptly to changes in temperature, levels of photosynthetically active radiation, and carbon dioxide[1,4]. These strong environmental controls link BVOC emission to the climate mean state and its variability[5-8]. Once emitted, BVOCs affect climate through various processes such as modifying the atmospheric oxidising capacity, which in turn changes the concentration of important greenhouse gases (i.e. ozone and methane), and contributing to secondary organic aerosol (SOA) formation[9]. Like all atmospheric aerosol, SOA alters the

radiative balance of the Earth both directly (through scattering and absorption of solar radiation) and indirectly (through changing cloud properties)[10,11]. In addition, atmospheric aerosol decreases the amount of radiation reaching the Earth surface, while concomitantly increasing its diffuse fraction. The vegetation response to this change in radiation regime is given by two competing effects on photosynthesis: inhibition due to reduction in total radiation and enhancement due to the diffuse radiation fertilisation effect[12-16]. The latter effect occurs because, under diffuse radiation conditions, light penetrates deeper into the canopy, illuminating leaves that may otherwise be in shade and thus enhancing photosynthesis overall. These interactions, together with the dominance of the SOA component in observed aerosol composition[17,18], point to the hitherto untested hypothesis that global BVOC emissions feedback on terrestrial primary production by SOA-induced changes in radiation quality and quantity. While this feedback has previously been identified regionally using observations from a boreal forest site[19], it has not yet been quantified at a global scale.

In this study we quantify the impact of biogenic SOA on terrestrial net primary productivity (NPP) through changes in direct and diffuse radiation at the surface. We use a modelling framework based on a combination of a global aerosol model[20], a radiation model[21], and a land surface scheme[16] (see Methods), previously used to quantify the response of plant photosynthesis to Amazonian biomass burning[15] and global fossil fuel burning[22].

The effect of biogenic secondary organic aerosol on radiation

To isolate the effect of biogenic SOA on radiation and plant productivity, we contrast simulations with and without BVOC emissions, holding other emissions of natural and anthropogenic primary aerosol, anthropogenic secondary aerosol source gases and concentrations of greenhouse gases at

present-day values. Current understanding of the global SOA production rate remains poor due to uncertainties in anthropogenic and biogenic VOC sources and emission rates, as well as the process of SOA formation. Here we focus on the biosphere-atmosphere interactions resulting from the emission of biogenic VOCs, and subsequent SOA formation. Previous estimates of global present-day isoprene emission range from 309–706 Tg C a^{-1} whilst total monoterpene emissions have been estimated at between 30–156 Tg C a^{-1} [23-25]. These wide ranges reflect differences in BVOC emission algorithms, as well as model representations of leaf area index, the distribution of plant functional types, and the driving meteorology. Accordingly, aerosol models give a wide range of global SOA formation totals with best estimates ranging between 13-121 Tg SOA a^{-1} according to a large intercomparison study[26]. To capture the uncertainties associated with BVOC emission and SOA production, we performed a series of sensitivity experiments that cover a range of global SOA production totals (17-100 Tg a^{-1}), together with an additional simulation using the GEOS-Chem model[27] (17 Tg a^{-1}) which includes a more complex treatment of SOA formation[28,29] (see Methods). We assess the ability of our modelling framework to capture the extent to which SOA alters the radiation regime by comparing against aerosol optical depth (AOD) observations. Figure 1a shows the simulated AOD against measurements at various AERONET sites with substantial BVOC emissions (see Methods, Supplementary Figure 1). We find the best agreement with observed AOD for simulations with a biogenic SOA source of between 34 Tg a^{-1} (1×SOA, Normalised Mean Bias, NMB=-14%) and 67 Tg a^{-1} (2×SOA, NMB=10%), consistent with previous evaluations of the biogenic SOA source in our model[11]. We use these two simulations as lower and upper bound estimates of SOA yields, and 50 Tg a^{-1} (1.5×SOA, NMB=0%) as our best estimate. This range encompasses the AOD simulated in our additional GEOS-Chem simulation (NMB=-6%) and is also in good agreement with the AeroCom models that parameterise SOA chemical production (median of 51 Tg a^{-1}, mean of 59 Tg a^{-1} with standard deviation of 38 Tg a^{-1})[26]. We obtain a similar best

estimate for SOA yield if we restrict our evaluation to tropical and sub-tropical latitudes (30°N-30°S) (Figure 1b and Supplementary Figure 2).

The effect of biogenic SOA on surface short-wave radiation in our best estimate simulation is shown in Figure 2 (and is consistent with the effects estimated in the additional GEOS-Chem simulation, Supplementary Figure 3). The presence of SOA in the atmosphere leads to a 0.03% global mean decrease in total surface radiation (annual global mean of -0.08 Wm^{-2}, Figure 2a), which largely results from a more pronounced decrease in direct radiation (annual global mean of -1.09 Wm^{-2}, Figure 2b). However, the presence of SOA in the atmosphere also leads to an increase in diffuse radiation (annual global mean of 1.01 Wm^{-2}, Figure 2c). As expected from the geographical distribution of BVOC emissions[1], the rate of formation of SOA from BVOCs and the lifetime of SOA in the atmosphere, the largest effect is in the tropics, with transfer of direct radiation to diffuse radiation reaching ~10 Wm^{-2} over South America and central Africa.

Vegetation response to surface radiation changes

The changes in the surface radiation regime driven by biogenic SOA affect land vegetation via the diffuse radiation fertilisation effect[12-16], thus altering gross primary productivity (GPP) and net primary productivity (NPP). Figure 3a shows the simulated impact on NPP; we estimate that SOA leads to NPP increases over most of the globe, with regional increases of up to 0.2 gC m^{-2} day^{-1} in parts of South America, central Africa and Indonesia. While modest NPP decreases are simulated in a few regions where the inhibition of photosynthesis caused by the decrease in direct radiation dominates over the diffuse radiation fertilisation effect (e.g. high northern latitudes), the large NPP increases elsewhere result in an integrated annual mean global NPP enhancement of 1.23 Pg C a^{-1}

(0.76-1.61 Pg C a^{-1} range, when allowing for uncertainties in SOA yield, encompassing the 0.96 Pg C a^{-1} value simulated in the additional GEOS-Chem simulation). This corresponds to ~1.7% (range 1.0-2.2%) of the total NPP simulated in our model, i.e. 74 Pg C a^{-1}, within the 52-76 Pg C a^{-1} multi-model range from nine Dynamic Global Vegetation Models[30]. Most of the NPP enhancement comes from lower latitudes (30°N-30°S), which dominate the increases throughout the year, with smaller contributions from higher latitude regions (Figure 3b). The annual cycle reflects the contrast in land surface area between hemispheres; the smallest NPP increase is recorded in February and the largest in August, partly due to a substantial contribution from mid 30°-60° (30%) and boreal 60°N-90°N (10%) latitudes (Figure 3b).

Remarkably, this 1.23 Pg C a^{-1} increase in NPP is approximately 30 times larger than the SOA causing it (which is 50 Tg SOA a^{-1} or 40 Tg C a^{-1}) and approximately twice the 603 Tg C a^{-1} of BVOC source (513 Tg C a^{-1} isoprene and 90 Tg C a^{-1} monoterpenes, see Methods) that is responsible for forming the SOA. This means that at the global scale the terrestrial biosphere benefits from emission of BVOC, with an NPP enhancement that is twice as large as the initial carbon investment into the atmosphere. The ratio between the NPP enhancement and BVOC emissions (i.e. the efficiency of this return on the carbon investment in BVOC) is larger than 1 at most latitudes (Figure 3c), reaching values of ~10 in some areas such as the Great Lakes region of North America and central Africa (Figure 3d).

The change in diffuse to total radiation caused by biogenic SOA primarily drives an increase in gross primary productivity (GPP), and this follows a similar geographical pattern as the NPP enhancement (Supplementary Figure 4). The regional GPP changes due to biogenic SOA are of the same order of

magnitude with those driven by diffuse radiation fertilisation due to present day levels of anthropogenic pollution aerosol (Supplementary Figure 5). This effect from pollution aerosol[16], estimated here by contrasting present-day and pre-industrial aerosol simulations, is found to be in good agreement with recent work[31] based on results from a global Earth system model, where a 2% global GPP increase (with increases of up to 8% in some key regions such as North America and Eurasia) was estimated due to pollution aerosol.

Emissions of BVOCs and biogenic SOA formation are sensitive to increasing atmospheric CO_2 concentrations[32,33] and to future climate and land-use change[5-7,34]. Previous work estimated that changes in climate and CO_2 concentrations between 2000 and 2100 could lead to an 18% increase in SOA production rate[34]. Using a series of experiments investigating the sensitivity of NPP enhancement due to diffuse radiation fertilisation on a range of biogenic SOA production rates (see Methods), we estimate that an 18% increase in SOA production rate leads to an additional NPP enhancement from diffuse radiation fertilisation of 0.22 Pg C a^{-1}. This is equivalent to approximately 2.3% of the 9.4±0.5 Pg C a^{-1} fossil fuel and other industrial emissions in 2016[35]. In contrast, nutrient limitations[36,37] and future land-use change[5,34] will likely have an opposite effect, inhibiting SOA formation. This suggests that diffuse radiation fertilisation from biogenic SOA may play a modest role in future carbon sequestration. We also note that our evaluation of AOD helps to constrain uncertainties in SOA formation as well as aerosol lifetime, SOA burden and aerosol optical properties. Additional complexities in the response of vegetation to changing levels of direct and diffuse radiation (e.g. variability in canopy structure, changes in plant species, efficiency of scattering by SOA) are not explored, meaning that the full uncertainty range may be larger than calculated here.

Global feedback between plant emissions and plant productivity

Our modelling study provides a first global quantification of the positive feedback loop in the Earth system in which vegetation expends carbon that, mediated by atmospheric chemistry and physics, enhances its primary productivity. This feedback loop is part of the continental biosphere-aerosol-cloud-climate feedback mechanism[19], previously estimated to cause a regional gain in GPP of 1.3 (range 1.02-1.5)[19] for boreal forest ecosystems. We calculate that a 10% increase in global BVOC emissions results in a 2.1% increase in global terrestrial mean AOD, a 0.2% increase in global terrestrial mean diffuse fraction, a 0.08% increase in global GPP (0.13% in NPP), and finally a 0.73% increase in BVOC emissions (Figure 4). Thus we estimate that this feedback loop leads to a gain in global BVOC emissions of 1.07, within the range estimated by the previous regional-scale study. Our estimated feedback is dampened by approximately a factor 5 reduction in sensitivity between BVOC emissions and AOD (from 10% to 2.1%, due to the contribution of other aerosol sources to AOD) and a factor 10 reduction in sensitivity between AOD and diffuse fraction (from 2.1% to 0.2%, due to the dominant role of clouds). The magnitude of this feedback is also likely to rise as global climate warms and anthropogenic aerosol emissions decline. We note that other contributing effects of biogenic SOA which are not included here, such as aerosol cloud albedo[10,11] and lifetime effects, or aerosol-induced reductions in temperature[38], will affect the actual strength of this feedback. While our offline modelling framework cannot account fully for all these interactions, a sensitivity simulation with an imposed reduction in surface temperature (see Methods) indicates that the dominant effect in this feedback loop is the diffuse radiation fertilisation effect (Supplementary Table 1). Thus, we argue that future assessments of the terrestrial carbon sink within fully coupled Earth system models should account for the diffuse radiation fertilisation effect from biogenic SOA.

References

1 Guenther, A. *et al.* A global model of natural volatile organic compound emissions. *Journal of Geophysical Research: Atmospheres* **100**, 8873-8892, doi:10.1029/94JD02950 (1995).

2 Carslaw, K. S. *et al.* A review of natural aerosol interactions and feedbacks within the Earth system. *Atmos. Chem. Phys.* **10**, 1701-1737, doi:10.5194/acp-10-1701-2010 (2010).

3 Arneth, A. *et al.* Terrestrial biogeochemical feedbacks in the climate system. *Nature Geosci* **3**, 525-532 (2010).

4 Niinemets, Ü., Tenhunen, J. D., Harley, P. C. & Steinbrecher, R. A model of isoprene emission based on energetic requirements for isoprene synthesis and leaf photosynthetic properties for Liquidambar and Quercus. *Plant, Cell & Environment* **22**, 1319-1335, doi:10.1046/j.1365-3040.1999.00505.x (1999).

5 Heald, C. L. *et al.* Predicted change in global secondary organic aerosol concentrations in response to future climate, emissions, and land use change. *Journal of Geophysical Research: Atmospheres* **113**, D05211, doi:10.1029/2007JD009092 (2008).

6 Peñuelas, J. & Staudt, M. BVOCs and global change. *Trends in Plant Science* **15**, 133-144 (2010).

7 Paasonen, P. *et al.* Warming-induced increase in aerosol number concentration likely to moderate climate change. *Nature Geosci* **6**, 438-442, doi:10.1038/ngeo1800 (2013).

8 Laothawornkitkul, J., Taylor, J. E., Paul, N. D. & Hewitt, C. N. Biogenic volatile organic compounds in the Earth system. *New Phytologist* **183**, 27-51, doi:10.1111/j.1469-8137.2009.02859.x (2009).

9 Scott, C. E. *et al.* Impact on short-lived climate forcers increases projected warming due to deforestation. *Nature Communications* **9**, 157, doi:10.1038/s41467-017-02412-4 (2018).

10 Rap, A. *et al.* Natural aerosol direct and indirect radiative effects. *Geophysical Research Letters* **40**, 3297-3301, doi:10.1002/grl.50441 (2013).

11 Scott, C. E. *et al.* The direct and indirect radiative effects of biogenic secondary organic aerosol. *Atmospheric Chemistry and Physics* **14**, 447-470, doi:10.5194/acp-14-447-2014 (2014).

12 Roderick, M. L., Farquhar, G. D., Berry, S. L. & Noble, I. R. On the direct effect of clouds and atmospheric particles on the productivity and structure of vegetation. *Oecologia* **129**, 21-30, doi:10.1007/s004420100760 (2001).

13 Gu, L. H. *et al.* Response of a deciduous forest to the Mount Pinatubo eruption: Enhanced photosynthesis. *Science* **299**, 2035-2038, doi:10.1126/science.1078366 (2003).

14 Cirino, G. G., Souza, R. A. F., Adams, D. K. & Artaxo, P. The effect of atmospheric aerosol particles and clouds on net ecosystem exchange in the Amazon. *Atmos. Chem. Phys.* **14**, 6523-6543, doi:10.5194/acp-14-6523-2014 (2014).

15 Rap, A. *et al.* Fires increase Amazon forest productivity through increases in diffuse radiation. *Geophysical Research Letters* **42**, 4654-4662, doi:10.1002/2015GL063719 (2015).

16 Mercado, L. M. *et al.* Impact of changes in diffuse radiation on the global land carbon sink. *Nature* **458**, 1014-U1087, doi:10.1038/nature07949 (2009).

17 Zhang, Q. *et al.* Ubiquity and dominance of oxygenated species in organic aerosols in anthropogenically-influenced Northern Hemisphere midlatitudes. *Geophysical Research Letters* **34**, L13801, doi:10.1029/2007GL029979 (2007).

18 Jimenez, J. L. *et al.* Evolution of Organic Aerosols in the Atmosphere. *Science* **326**, 1525-1529, doi:10.1126/science.1180353 (2009).

19 Kulmala, M. N., Tuomo; Nikandrova, Anna; Lehtipalo, Katrianne; Manninen, Hanna E.; Kajos, Maija K.; Kolari, Pasi; Lauri, Antti; Petaja, Tuukka; Krejci, Radovan; Hansson, Hans-Christen; Swietlicki, Erik; Lindroth, Anders; Christensen, Torben R.; Arneth, Almut; Hari, Pertti; Back, Jaana; Vesala, Timo; Kerminen, Veli-Matti. CO2-induced terrestrial climate feedback mechanism : From carbon sink to aerosol source and back. *Boreal Environment Research* **19**, 122-131 (2014).

20 Mann, G. W. *et al.* Description and evaluation of GLOMAP-mode: a modal global aerosol microphysics model for the UKCA composition-climate model. *Geoscientific Model Development* **3**, 519-551, doi:10.5194/gmd-3-519-2010 (2010).
21 Edwards, J. M. & Slingo, A. Studies with a flexible new radiation code .1. Choosing a configuration for a large-scale model. *Quarterly Journal of the Royal Meteorological Society* **122**, 689-719, doi:10.1002/qj.49712253107 (1996).
22 O'Sullivan, M. *et al.* Small global effect on terrestrial net primary production due to increased fossil fuel aerosol emissions from East Asia since the turn of the century. *Geophysical Research Letters* **43**, 8060-8067, doi:10.1002/2016GL068965 (2016).
23 Arneth, A., Monson, R. K., Schurgers, G., Niinemets, Ü. & Palmer, P. I. Why are estimates of global terrestrial isoprene emissions so similar (and why is this not so for monoterpenes)? *Atmos. Chem. Phys.* **8**, 4605-4620, doi:10.5194/acp-8-4605-2008 (2008).
24 Schurgers, G., Arneth, A., Holzinger, R. & Goldstein, A. H. Process-based modelling of biogenic monoterpene emissions combining production and release from storage. *Atmos. Chem. Phys.* **9**, 3409-3423, doi:10.5194/acp-9-3409-2009 (2009).
25 Guenther, A. B. *et al.* The Model of Emissions of Gases and Aerosols from Nature version 2.1 (MEGAN2.1): an extended and updated framework for modeling biogenic emissions. *Geosci. Model Dev.* **5**, 1471-1492, doi:10.5194/gmd-5-1471-2012 (2012).
26 Tsigaridis, K. *et al.* The AeroCom evaluation and intercomparison of organic aerosol in global models. *Atmos. Chem. Phys.* **14**, 10845-10895, doi:10.5194/acp-14-10845-2014 (2014).
27 Bey, I. *et al.* Global modeling of tropospheric chemistry with assimilated meteorology: Model description and evaluation. *Journal of Geophysical Research: Atmospheres* **106**, 23073-23095, doi:10.1029/2001JD000807 (2001).
28 Liao, H., Henze, D. K., Seinfeld, J. H., Wu, S. & Mickley, L. J. Biogenic secondary organic aerosol over the United States: Comparison of climatological simulations with observations. *Journal of Geophysical Research: Atmospheres* **112**, D06201, doi:10.1029/2006JD007813 (2007).
29 Pye, H. O. T., Chan, A. W. H., Barkley, M. P. & Seinfeld, J. H. Global modeling of organic aerosol: the importance of reactive nitrogen (NO_x and NO₃). *Atmos. Chem. Phys.* **10**, 11261-11276, doi:10.5194/acp-10-11261-2010 (2010).
30 Sitch, S. *et al.* Recent trends and drivers of regional sources and sinks of carbon dioxide. *Biogeosciences* **12**, 653-679, doi:10.5194/bg-12-653-2015 (2015).
31 Strada, S. & Unger, N. Potential sensitivity of photosynthesis and isoprene emission to direct radiative effects of atmospheric aerosol pollution. *Atmos. Chem. Phys.* **16**, 4213-4234, doi:10.5194/acp-16-4213-2016 (2016).
32 Arneth, A. *et al.* Process-based estimates of terrestrial ecosystem isoprene emissions: incorporating the effects of a direct CO₂-isoprene interaction. *Atmos. Chem. Phys.* **7**, 31-53, doi:10.5194/acp-7-31-2007 (2007).
33 Unger, N. Isoprene emission variability through the twentieth century. *Journal of Geophysical Research: Atmospheres* **118**, 13,606-613,613, doi:10.1002/2013JD020978 (2013).
34 Lin, G., Penner, J. E. & Zhou, C. How will SOA change in the future? *Geophysical Research Letters* **43**, 1718-1726, doi:10.1002/2015GL067137 (2016).
35 Le Quéré, C. *et al.* Global Carbon Budget 2017. *Earth Syst. Sci. Data Discuss.* **2017**, 1-79, doi:10.5194/essd-2017-123 (2017).
36 Fisher, J. B., Badgley, G. & Blyth, E. Global nutrient limitation in terrestrial vegetation. *Global Biogeochemical Cycles* **26**, GB3007, doi:10.1029/2011GB004252 (2012).
37 Norby, R. J. *et al.* Model–data synthesis for the next generation of forest free-air CO2 enrichment (FACE) experiments. *New Phytologist* **209**, 17-28, doi:10.1111/nph.13593 (2016).
38 Doughty, C. E., Flanner, M. G. & Goulden, M. L. Effect of smoke on subcanopy shaded light, canopy temperature, and carbon dioxide uptake in an Amazon rainforest. *Global Biogeochemical Cycles* **24**, doi:10.1029/2009gb003670 (2010).

Corresponding author: Alexandru Rap (a.rap@leeds.ac.uk)

Acknowledgements We acknowledge funding from the Natural Environment Research Council (NE/J004723/1, NE/J009822/1 and NE/K015966/1) and EU Horizon 2020 (SC5-01-2014; grant agreement 641816). D.V.S. acknowledges support from a Philip Leverhulme Prize. We thank the modellers from the TRENDY multi-model intercomparison project for access to their DGVM output and the principal investigators and their staff for establishing and maintaining the AERONET sites used in this study. We also thank Andrew Jarvis for initial discussions and Natalia Restrepo-Coupe and Damien Bonal for access to the data used in Supplementary Information Figure 7.

Author Contributions A.R., D.J.B, A.R.M., C.N.H. and D.V.S. contributed to the design of the study. A.R., C.E.S., C.L.R., and D.V.S. analysed and interpreted the results. A.R. performed the radiation and land-surface modelling. C.E.S. performed the aerosol modelling. C.L.R. analysed the AERONET data. L.M. and R.J.E. developed the land-surface modelling framework. S.G. and M.J.E. provided the GEOS-Chem simulation. All authors contributed to scientific discussions and commented on the manuscript.

Competing Financial Interests statement The authors declare no competing financial interests.

Data availability. The AERONET remote-sensed data are publicly available from https://aeronet.gsfc.nasa.gov/. Data from our model simulations are available from the corresponding author upon request.

Code availability. Requests for the radiative transfer and land-surface models used to generate these results can be made via https://code.metoffice.gov.uk/trac/home and http://jules.jchmr.org/, respectively.

Figure captions

Figure 1. Comparison of monthly-mean simulated AOD against AERONET observations. (a) Modelled vs. observed AOD values from 23 AERONET sites located in regions with large BVOC emissions in South America, Africa, North America and Europe (see Methods; site locations shown in Figure 2c); lines of best fit (least absolute deviation method) and normalized mean biases (NMB) are included. (b) Box plot of modelled and observed AOD from the subset of 9 AERONET sites located between 30°N-30°S (boxes show medians and 25-75% interquartile ranges, asterisks means, and whiskers minimum-maximum ranges). The colours correspond to the seven simulations (see Methods): no SOA (grey), 17 Tg SOA a^{-1} (0.5×SOA, orange), 34 Tg SOA a^{-1} (1×SOA, red), 50 Tg SOA a^{-1} (1.5×SOA, blue), 67 Tg SOA a^{-1} (2×SOA, green), 100 Tg SOA a^{-1} (3×SOA, cyan) and GEOSChem (magenta).

Figure 2. Simulated impact of biogenic SOA on surface radiation. Annual mean changes in (a) total, (b) direct, and (c) diffuse solar radiation at the surface [W m^{-2}] caused by the 50 Tg a^{-1} (1.5×SOA) biogenic SOA source. Values above panels are global averages. The blue crosses in panel (c) show locations of the observation sites used in Figures 1 and Supplementary Figure 1. Hatches show areas where the changes are significant to the 95% confidence level.

Figure 3. Simulated diffuse radiation fertilisation effect caused by the 50 Tg a^{-1} biogenic SOA source. (a) Annual mean ΔNPP [in gC m^{-2} day^{-1}], with hatches showing areas where the changes are significant to the 95% confidence level. (b) Monthly mean global NPP enhancement [in Tg C] for different latitudinal bands (error bars correspond to the uncertainty in SOA formation). (c) Zonal

mean BVOC emissions and ΔNPP [in gC m^{-2} day^{-1}] (black lines) and their ratio ΔNPP/BVOC (blue line). (d) Distribution of the annual mean ratio between ΔNPP and BVOC emissions.

340

Figure 4. Simulated global feedback loop between plant emissions and plant productivity. A 10% increase in biogenic volatile organic compounds (BVOC) emissions, leads to increases of 2.1% in global terrestrial aerosol optical depth (AOD), 0.2% increase in global terrestrial diffuse fraction (i.e. the fraction between diffuse and total surface radiation), 0.08% increase gross primary productivity
345 (GPP), and a 0.73% increase in BVOC emissions. This corresponds to a 1.07 gain in BVOC emissions resulting from this feedback loop.

Methods

Aerosol model. The mass and number of size resolved atmospheric aerosol particles were simulated with the modal version of the 3-D GLObal Model of Aerosol Processes (GLOMAP-mode)[20,39,40], which is an extension to the TOMCAT chemical transport model[41]. TOMCAT is driven by analysed meteorology (ERA-Interim) from the European Centre for Medium-Range Weather Forecasts (ECMWF), updated every 6 hours and linearly interpolated onto the model time-step. Our simulations are performed for the year 2000 (i.e., one year duration), with 6 months spin-up. The horizontal resolution of the model is 2.8º×2.8º, with 31 vertical model levels between the surface and 10 hPa and 6 vertical levels within the lowest 1.5 km of atmosphere (approximately encompassing the convective boundary layer). The aerosol size distribution is treated using a two-moment modal scheme with 5 modes: hydrophilic nucleation, Aitken, accumulation and coarse modes and non-hydrophilic Aitken mode[20]. The aerosol species included in GLOMAP are black carbon (BC), particulate organic matter (POM), sulphate and sea salt. Within each mode the different aerosol components are internally mixed. GLOMAP includes representations of nucleation, particle growth via coagulation, condensation and cloud processing, wet and dry deposition, and scavenging. This configuration of GLOMAP-mode includes annual mean emissions of BC and POM from fossil and biofuel combustion[42], monthly biomass burning emissions of BC and POM for the year 2000 from the Global Fire Emissions Database (GFEDv3) inventory[43] and parameterised[44] emission of primary sea-salt aerosol. We prescribe six-hourly mean offline oxidant (OH, O_3, NO_3, HO_2, H_2O_2) concentrations from a previous TOMCAT simulation[45]. Emissions of monoterpenes and isoprene are simulated for the year 2000 using the BVOC model[46] inside the Joint UK Land Environment Simulator (JULES) land surface model[47,48], giving total global emissions of 90 and 513 Tg C a^{-1}, respectively. A gas-phase secondary organic species is generated at fixed molar yields of 13% and 3% from the oxidation (by O_3, NO_3 and OH) of monoterpenes and isoprene respectively;

monoterpenes are modelled using reaction rates characteristic of α-pinene. We assume that BVOCs oxidise to form non-volatile organic material which condenses irreversibly onto existing aerosol according to their Fuchs-Sutugin corrected surface area[49]; we examine the sensitivity of radiative effects to this approach elsewhere[50]. GLOMAP includes phytoplankton emissions of dimethyl-
375 sulphide (DMS), calculated using monthly sea-water DMS concentrations[51], and gas-phase sulphur dioxide (SO_2) emissions from anthropogenic sources[52], biomass burning[43], and both continuous[53] and explosive[54] volcanic eruptions.

The additional GEOS-Chem[27] (v11-01) simulation was run at the 2º×2.5º resolution, with 47 vertical layers using the NOx-Ox-hydrocarbon-aerosol-bromine tropospheric chemistry mechanism
380 (tropchem). The SOA scheme[28,29] uses lumped oxidation products, with SOA formation rates derived from experimentally determined rate constant and aerosol yield parameters. The tropchem mechanism covers NOx-Ox-hydrocarbon chemistry in the troposphere, including both kinetic and photolysis reactions. The reaction rates were calculated using experimentally derived rate constants and photolysis cross sections; the combined tropchem + SOA simulation includes 95 advected
385 species. The simulations were run using Global Modeling and Assimilation Office (GMAO) Goddard Earth Observing System Forward Processing (GEOS-FP) meteorology.

Aerosol output fields from both GLOMAP and GEOS-Chem simulations are coupled off-line to the SOCRATES radiative transfer model.

Radiative transfer model. The aerosol effect on direct and diffuse radiation was calculated at each
390 model level using output from the aerosol model and the SOCRATES radiative transfer model[10,21] with six bands in the short-wave and nine bands in the long-wave, based on the two-stream equations at all wavelengths. The surface diffuse radiation flux available for photosynthesis was obtained by subtracting the direct flux (calculated using an Eddington two-stream scattering solver) from the total flux (calculated using a delta-Eddington solver). Aerosol optical properties were calculated for all

aerosol modes using RADAER[55]. Due to the optical properties prescribed to SOA particles in our model, together with their size and location, most SOA scattering occurs in the forward direction, leading to a relatively low annual global mean upscatter fraction of 0.07. For comparison, the upscatter fraction of anthropogenic aerosol in our model is 0.28, within the 0.17-0.29 range from existing estimates[56]. We used a monthly mean climatology for water vapour, temperature and ozone based on ECMWF reanalysis data, together with surface albedo and cloud optical depth fields from the International Satellite Cloud Climatology Project (ISCCP)-D2[57]. Previous work has shown that aerosol radiative effects simulated using the SOCRATES radiative transfer model combined with the GLOMAP aerosol model are in good agreement with other estimates of observed and modelled effects for both natural[10,11,15] and anthropogenic[58,59] aerosols. We have also found our model's partitioning of diffuse/direct radiation caused by year 2000 biomass burning aerosol (Supplementary Figure 6) to be in good agreement with results from NASA E2-YIBs Earth System model simulations[31].

Radiation output fields from SOCRATES simulations are coupled off-line to the JULES land surface model.

Land-surface model. The Joint UK Land Environment Simulator (JULES) land surface model represents the fluxes of water, energy and carbon between the land and the atmosphere[47,48]. This study uses the canopy radiation-photosynthesis scheme in JULES version 3.2 that accounts for effects of diffuse radiation on sunlit and shaded photosynthesis[16,60]. The model is run with a temporal resolution of three hours and a spatial resolution of 0.5º×0.5º across the domain and forced with meteorological driving data. The meteorological components consist of 2 m air temperature and specific humidity, precipitation, 10 m wind speed and surface pressure. The data were derived using the methodology for bias correction[61] of the ERA Interim reanalysis product. The model uses

downward direct and diffuse short-wave and long-wave radiation at the surface, derived from our radiative transfer model, as shown in Figure 2. The soil hydrology utilises the van Genuchten relationships[62] and parameters derived from the Harmonised World Soil Database[63]. The BVOC emissions simulated interactively in the model[46] are based on a semi-mechanistic isoprene emission module[4,32] and a semi-empirical approach for monoterpenes. We use the following PFT-specific emission factors for broad-leaf trees, needle-leaf trees, C3 grass, C4 grass, and shrubs: 39, 14, 14, 14, and 23 μg g^{-1} h^{-1} for isoprene[46] and 1.39, 8.4, 1.4, 4.2, and 1.58 μg g^{-1} h^{-1} for monoterpene (based on existing monoterpene to isoprene emission factor ratios from the LPJ-GUESS model[64]). For the year 2000 simulated in this work, the global total monoterpene and isoprene emissions are 90 and 513 Tg C a^{-1} respectively, in good agreement with previous estimates of present-day BVOC emissions (i.e. 30 – 156 Tg C a^{-1} and 309 - 706 Tg C a^{-1} for monoterpenes and isoprene respectively)[23-25]. The JULES land surface scheme used here has previously been shown to reproduce the observed plant carbon uptake response to changes in direct and diffuse radiation at both tropical[15] and temperate[16,22] forest sites. The simulated enhancement of GPP as a function of diffuse fraction is also in good agreement with high-frequency flux data measurements from two South American sites[15,65,66] (Supplementary Figure 7).

Observations used in AOD evaluation. Simulated monthly mean AOD values at 505 nm were compared with corresponding Version 2 Level 2.0 cloud-screened and quality assured daytime average AOD retrieved at 500 nm using CIMEL sun-sky spectral radiometers at 23 stations in the Aerosol Robotic Network[67] (AERONET): Abracos Hill (10S,62W), Alta Floresta (9S,56W), Balbina (1S,59W), Rio Branco (9S,67W), and Santa Cruz (17S,63W) in South America; Ilorin (8N,4E), Mongu (15S,23E), and Skukuza (24S,31E) in Africa; Cart Site (36N,97W), Chequamegon (45N,90W), HJ Andrews (44N,122W), Howland (45N,68W), La Jolla (32N,117W), Maricopa (33N,111W), MD Science Center (39N,76W), Saturn Island (48N,123W), Sevilleta (34N,106W),

Sioux Falls (43N,96W), Stennis (30N,89W), Table Mountain (40N,105W), Tucson (32N,110W), Walker Branch (35N,84W) in North America; Gotland (57N,18E) in Europe. The AERONET AOD values used to evaluate the simulated AOD (and shown in Figure 1 and Supplementary Figures 1 and 2) are multi-annual monthly means calculated from all years of data available at each station. To minimise the effect of other aerosol (e.g. biomass burning, pollution aerosol), we only include values from January-June (South America, Mongu and Skukuza) and June-November (Ilorin, North America, and Europe) corresponding to AERONET sites where biogenic SOA contributes more than 20% of total simulated monthly mean AOD.

Simulations. Using emissions of isoprene (513 Tg C a^{-1}) and monoterpenes (90 Tg C a^{-1}) simulated interactively in the JULES land surface model, we performed several one-year simulations with the GLOMAP aerosol microphysics model: noSOA, with all BVOC emissions switched off; 0.5×SOA, 1×SOA, 1.5×SOA, 2×SOA, and 3×SOA, with SOA yield production (molar yields of 13% and 3% for the oxidation of monoterpenes and isoprene respectively) scaled by a factor of 0.5, 1, 1.5, 2, and 3, respectively. Our simulations represent the year 2000 and follow a 6 month spin-up period. An additional experiment using biogenic SOA simulated by the GEOS-Chem model[27-29] has also been performed to explore the uncertainty introduced by our SOA treatment. For each experiment, monthly-mean output from the aerosol model was combined with SOCRATES to determine changes to direct and diffuse shortwave radiation fluxes, relative to the noSOA simulation. These radiation fields are then used to drive the JULES land-surface model to determine changes in plant productivity and biogenic emissions. To investigate the gain in BVOC emissions resulted from the feedback between plant emissions and plant productivity, we performed an experiment with an artificial 10% increase in BVOC emissions (thus using of 565 Tg C a^{-1} isoprene and 99 Tg C a^{-1} of monoterpenes). Finally, to obtain a first order estimate of how this gain is affected by the aerosol induced reduction in surface temperature, an additional JULES simulation used a constant imposed

change in global surface temperature of -0.012 K (calculated by multiplying the -0.02 Wm^{-2} aerosol radiative effect due to the 10% BVOC emissions increase with the multi-model mean[68] aerosol transient climate sensitivity value of 0.595 K $W^{-1}m^2$).

Additional references used only in the Methods section

39 Spracklen, D. V., Pringle, K. J., Carslaw, K. S., Chipperfield, M. P. & Mann, G. W. A global off-line model of size-resolved aerosol microphysics: I. Model development and prediction of aerosol properties. *Atmospheric Chemistry and Physics* **5**, 2227-2252 (2005).

40 Spracklen, D. V., Pringle, K. J., Carslaw, K. S., Chipperfield, M. P. & Mann, G. W. A global off-line model of size-resolved aerosol microphysics: II. Identification of key uncertainties. *Atmos. Chem. Phys.* **5**, 3233-3250, doi:10.5194/acp-5-3233-2005 (2005).

41 Stockwell, D. Z. & Chipperfield, M. P. A tropospheric chemical-transport model: Development and validation of the model transport schemes. *Quarterly Journal of the Royal Meteorological Society* **125**, 1747-1783, doi:10.1002/qj.49712555714 (1999).

42 Bond, T. C. *et al.* A technology-based global inventory of black and organic carbon emissions from combustion. *Journal of Geophysical Research: Atmospheres* **109**, D14203, doi:10.1029/2003JD003697 (2004).

43 van der Werf, G. R. *et al.* Global fire emissions and the contribution of deforestation, savanna, forest, agricultural, and peat fires (1997-2009). *Atmospheric Chemistry and Physics* **10**, 11707-11735, doi:10.5194/acp-10-11707-2010 (2010).

44 Gong, S. L. A parameterization of sea-salt aerosol source function for sub- and super-micron particles. *Global Biogeochemical Cycles* **17**, 1097, doi:10.1029/2003GB002079 (2003).

45 Monks, S. A. *et al.* The TOMCAT global chemical transport model v1.6: description of chemical mechanism and model evaluation. *Geosci. Model Dev.* **10**, 3025-3057, doi:10.5194/gmd-10-3025-2017 (2017).

46 Pacifico, F. *et al.* Evaluation of a photosynthesis-based biogenic isoprene emission scheme in JULES and simulation of isoprene emissions under present-day climate conditions. *Atmos. Chem. Phys.* **11**, 4371-4389, doi:10.5194/acp-11-4371-2011 (2011).

47 Best, M. J. *et al.* The Joint UK Land Environment Simulator (JULES), model description - Part 1: Energy and water fluxes. *Geoscientific Model Development* **4**, 677-699, doi:10.5194/gmd-4-677-2011 (2011).

48 Clark, D. B. *et al.* The Joint UK Land Environment Simulator (JULES), model description - Part 2: Carbon fluxes and vegetation dynamics. *Geoscientific Model Development* **4**, 701-722, doi:10.5194/gmd-4-701-2011 (2011).

49 Fuchs, N. A. & Sutugin, A. G. in *Topics in Current Aerosol Research* (ed J. R. Brock) 1 (Pergamon, 1971).

50 Scott, C. E. *et al.* Impact of gas-to-particle partitioning approaches on the simulated radiative effects of biogenic secondary organic aerosol. *Atmos. Chem. Phys.* **15**, 12989-13001, doi:10.5194/acp-15-12989-2015 (2015).

51 Kettle, A. J. & Andreae, M. O. Flux of dimethylsulfide from the oceans: A comparison of updated data sets and flux models. *Journal of Geophysical Research: Atmospheres* **105**, 26793-26808, doi:10.1029/2000JD900252 (2000).

52 Cofala, J., Amann, M., Klimont, Z. S. & Schopp, W. Scenarios of World Anthropogenic Emissions of SO2, NOx and CO up to 2030. (International Institute for Applied Systems Analysis, Laxenburg, Austria, 2005).

53 Andres, R. J. & Kasgnoc, A. D. A time-averaged inventory of subaerial volcanic sulfur emissions. *Journal of Geophysical Research: Atmospheres* **103**, 25251-25261, doi:10.1029/98JD02091 (1998).
54 Halmer, M. M., Schmincke, H. U. & Graf, H. F. The annual volcanic gas input into the atmosphere, in particular into the stratosphere: a global data set for the past 100 years. *Journal of Volcanology and Geothermal Research* **115**, 511-528 (2002).
55 Bellouin, N. *et al.* Impact of the modal aerosol scheme GLOMAP-mode on aerosol forcing in the Hadley Centre Global Environmental Model. *Atmospheric Chemistry and Physics* **13**, 3027-3044, doi:10.5194/acp-13-3027-2013 (2013).
56 Penner, J. E. *et al.* Aerosols, their Direct and Indirect Effects. In J. T. Houghton, Y. Ding, D. J. Griggs, M. Noguer, P. J. van der Linden, X. Dai, et al. (Eds.), Climate Change 2001: The Scientific Basis. Contribution of Working Group I to the Third Assessment Report of the Intergovernmental Panel on Climate Change (pp. 289-348). Cambridge University Press (2001).
57 Rossow, W. B. & Schiffer, R. A. Advances in understanding clouds from ISCCP. *Bulletin of the American Meteorological Society* **80**, 2261-2287, doi:10.1175/1520-0477(1999)080<2261:aiucfi>2.0.co;2 (1999).
58 Butt, E. W. *et al.* The impact of residential combustion emissions on atmospheric aerosol, human health, and climate. *Atmos. Chem. Phys.* **16**, 873-905, doi:10.5194/acp-16-873-2016 (2016).
59 Kapadia, Z. Z. *et al.* Impacts of aviation fuel sulfur content on climate and human health. *Atmos. Chem. Phys.* **16**, 10521-10541, doi:10.5194/acp-16-10521-2016 (2016).
60 Mercado, L. M., Huntingford, C., Gash, J. H. C., Cox, P. M. & Jogireddy, V. Improving the representation of radiation interception and photosynthesis for climate model applications. *Tellus Series B-Chemical and Physical Meteorology* **59**, 553-565, doi:10.1111/j.1600-0889.2007.00256.x (2007).
61 Weedon, G. P. *et al.* Creation of the WATCH Forcing Data and Its Use to Assess Global and Regional Reference Crop Evaporation over Land during the Twentieth Century. *Journal of Hydrometeorology* **12**, 823-848, doi:10.1175/2011jhm1369.1 (2011).
62 van Genuchten, M. T. A CLOSED-FORM EQUATION FOR PREDICTING THE HYDRAULIC CONDUCTIVITY OF UNSATURATED SOILS. *Soil Science Society of America Journal* **44**, 892-898 (1980).
63 Harmonized World Soil Database (2012), HWSD/FAO/IIASA/ISRIC/ISSCAS/JRC, (Version 1.2), FAO, Rome and IIASA, Laxenburg, Austria.
64 Acosta Navarro, J. C. *et al.* Global emissions of terpenoid VOCs from terrestrial vegetation in the last millennium. *Journal of Geophysical Research: Atmospheres* **119**, 6867-6885, doi:10.1002/2013JD021238 (2014).
65 Restrepo-Coupe, N. *et al.* What drives the seasonality of photosynthesis across the Amazon basin? A cross-site analysis of eddy flux tower measurements from the Brasil flux network. *Agricultural and Forest Meteorology* **182–183**, 128-144 (2013).
66 Bonal, D. *et al.* Impact of severe dry season on net ecosystem exchange in the Neotropical rainforest of French Guiana. *Global Change Biology* **14**, 1917-1933, doi:10.1111/j.1365-2486.2008.01610.x (2008).
67 Holben, B. N. *et al.* AERONET - A federated instrument network and data archive for aerosol characterization. *Remote Sensing of Environment* **66**, 1-16, doi:10.1016/s0034-4257(98)00031-5 (1998).
68 Rotstayn, L. D., Collier, M. A., Shindell, D. T. & Boucher, O. Why Does Aerosol Forcing Control Historical Global-Mean Surface Temperature Change in CMIP5 Models? *Journal of Climate* **28**, 6608-6625, doi:10.1175/jcli-d-14-00712.1 (2015).

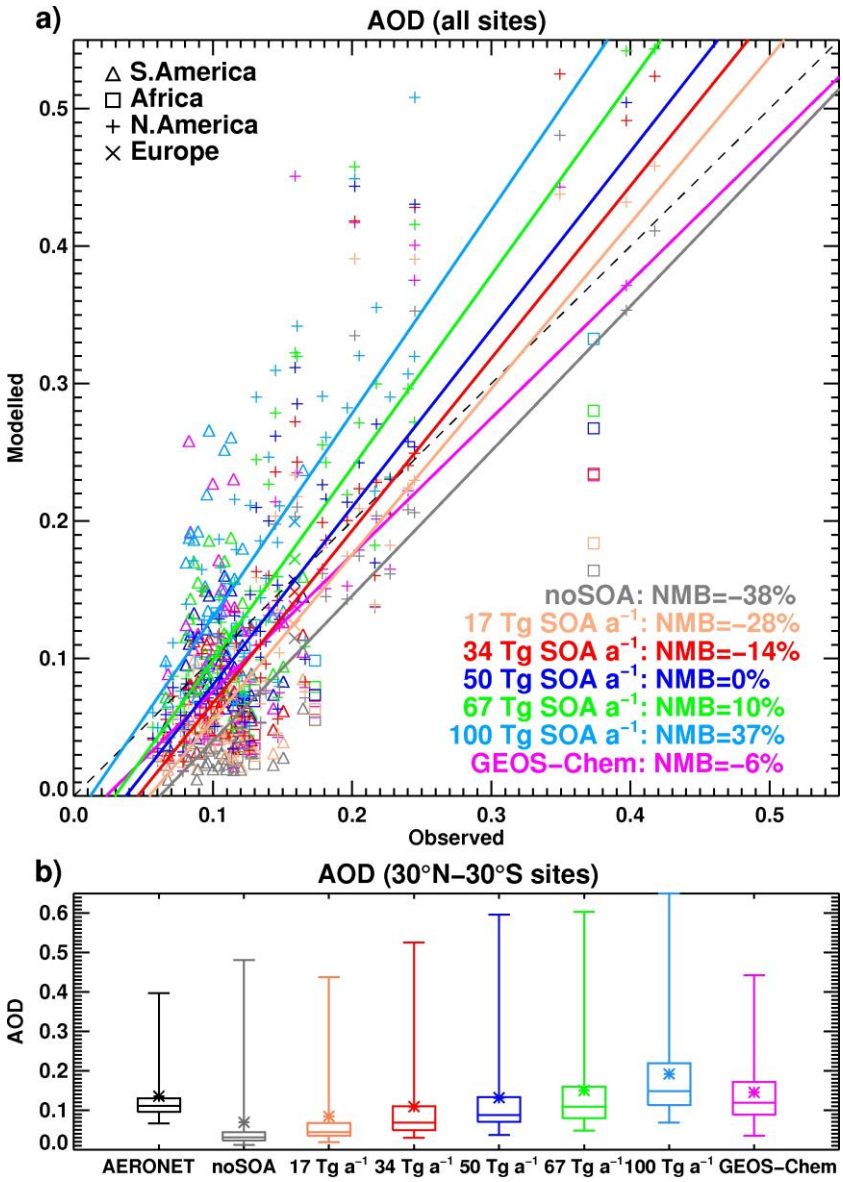

Figure 1. Comparison of monthly-mean simulated AOD against AERONET observations. (a) Modelled vs. observed AOD values from 23 AERONET sites located in regions with large BVOC emissions in South America, Africa, North America and Europe (see Methods; site locations shown in Figure 2c); lines of best fit (least absolute deviation method) and normalized mean biases (NMB) are included. (b) Box plot of modelled and observed AOD from the subset of 9 AERONET sites located between 30°N-30°S (boxes show medians and 25-75% interquartile ranges, asterisks means, and whiskers minimum-maximum ranges). The colours correspond to the seven simulations (see Methods): no SOA (grey), 17 Tg SOA a^{-1} (0.5×SOA, orange), 34 Tg SOA a^{-1} (1×SOA, red), 50 Tg SOA a^{-1} (1.5×SOA, blue), 67 Tg SOA a^{-1} (2×SOA, green), 100 Tg SOA a^{-1} (3×SOA, cyan) and GEOSChem (magenta).

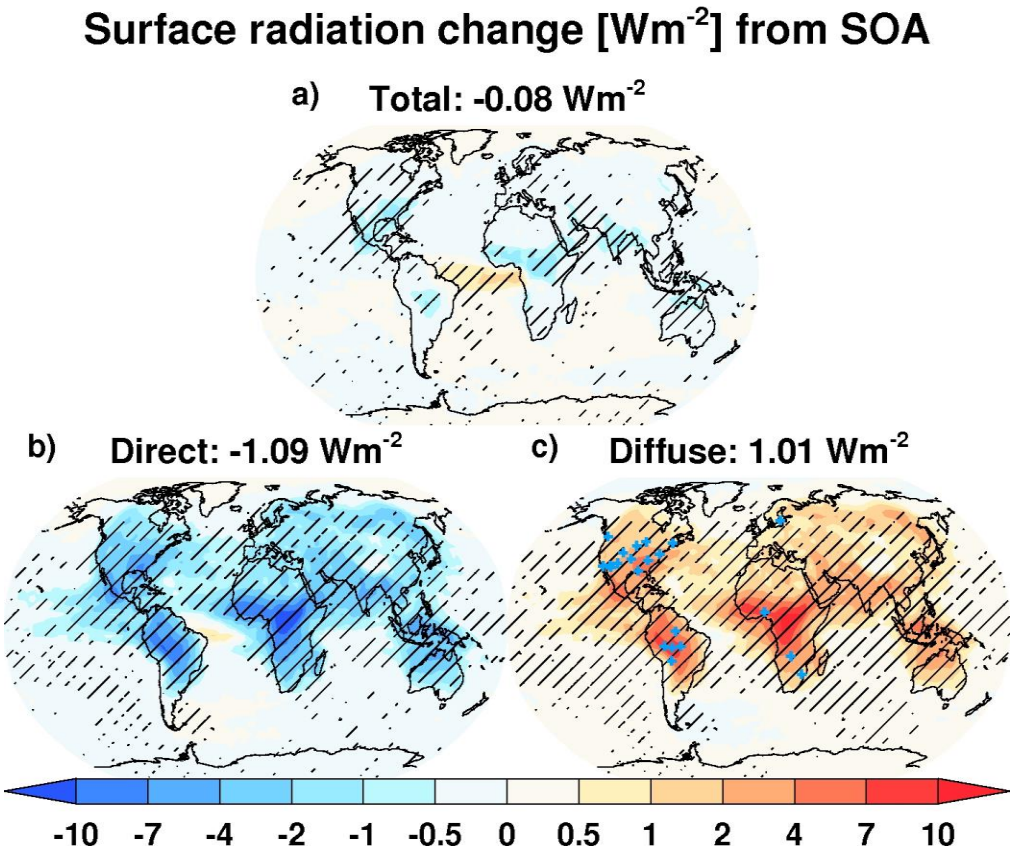

Figure 2. Simulated impact of biogenic SOA on surface radiation. Annual mean changes in (a) total, (b) direct, and (c) diffuse solar radiation at the surface [W m^{-2}] caused by the 50 Tg a^{-1} (1.5×SOA) biogenic SOA source. Values above panels are global averages. The blue crosses in panel (c) show locations of the observation sites used in Figures 1 and Supplementary Figure 1. Hatches show areas where the changes are significant to the 95% confidence level.

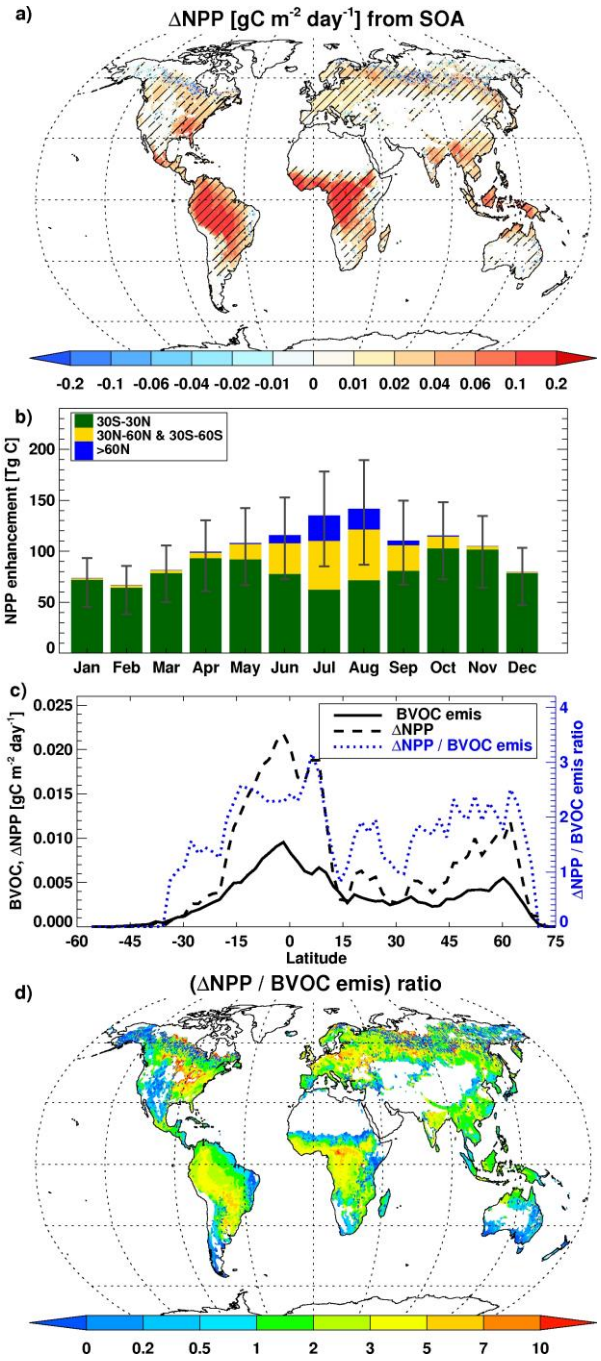

Figure 3. Simulated diffuse radiation fertilisation effect caused by the 50 Tg a^{-1} biogenic SOA source. (a) Annual mean ΔNPP [in gC m^{-2} day^{-1}], with hatches showing areas where the changes are significant to the 95% confidence level. (b) Monthly mean global NPP enhancement [in Tg C] for different latitudinal bands (error bars correspond to the uncertainty in SOA formation). (c) Zonal mean BVOC emissions and ΔNPP [in gC m^{-2} day^{-1}] (black lines) and their ratio ΔNPP/BVOC (blue line). (d) Distribution of the annual mean ratio between ΔNPP and BVOC emissions.

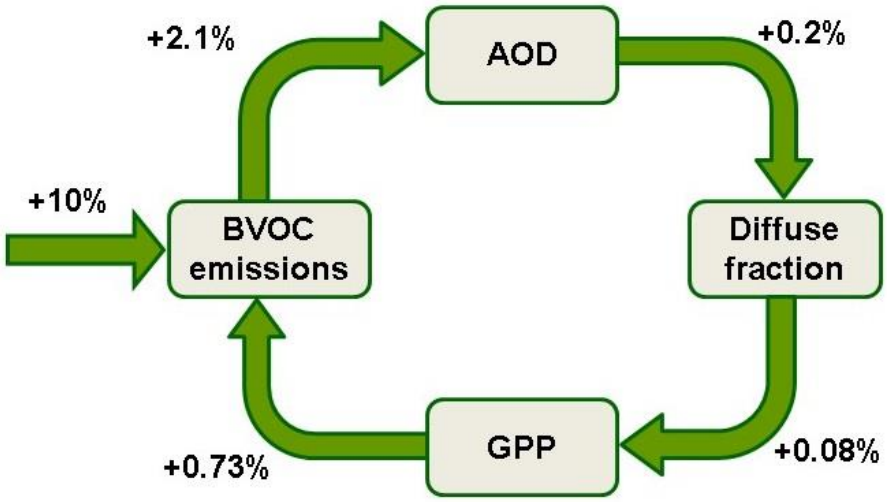

Figure 4. Simulated global feedback loop between plant emissions and plant productivity. A 10% increase in biogenic volatile organic compounds (BVOC) emissions, leads to increases of 2.1% in global terrestrial aerosol optical depth (AOD), 0.2% increase in global terrestrial diffuse fraction (i.e. the fraction between diffuse and total surface radiation), 0.08% increase gross primary productivity (GPP), and a 0.73% increase in BVOC emissions. This corresponds to a 1.07 gain in BVOC emissions resulting from this feedback loop.

Enhanced global primary production by biogenic aerosol via diffuse radiation fertilisation

Supplementary Information

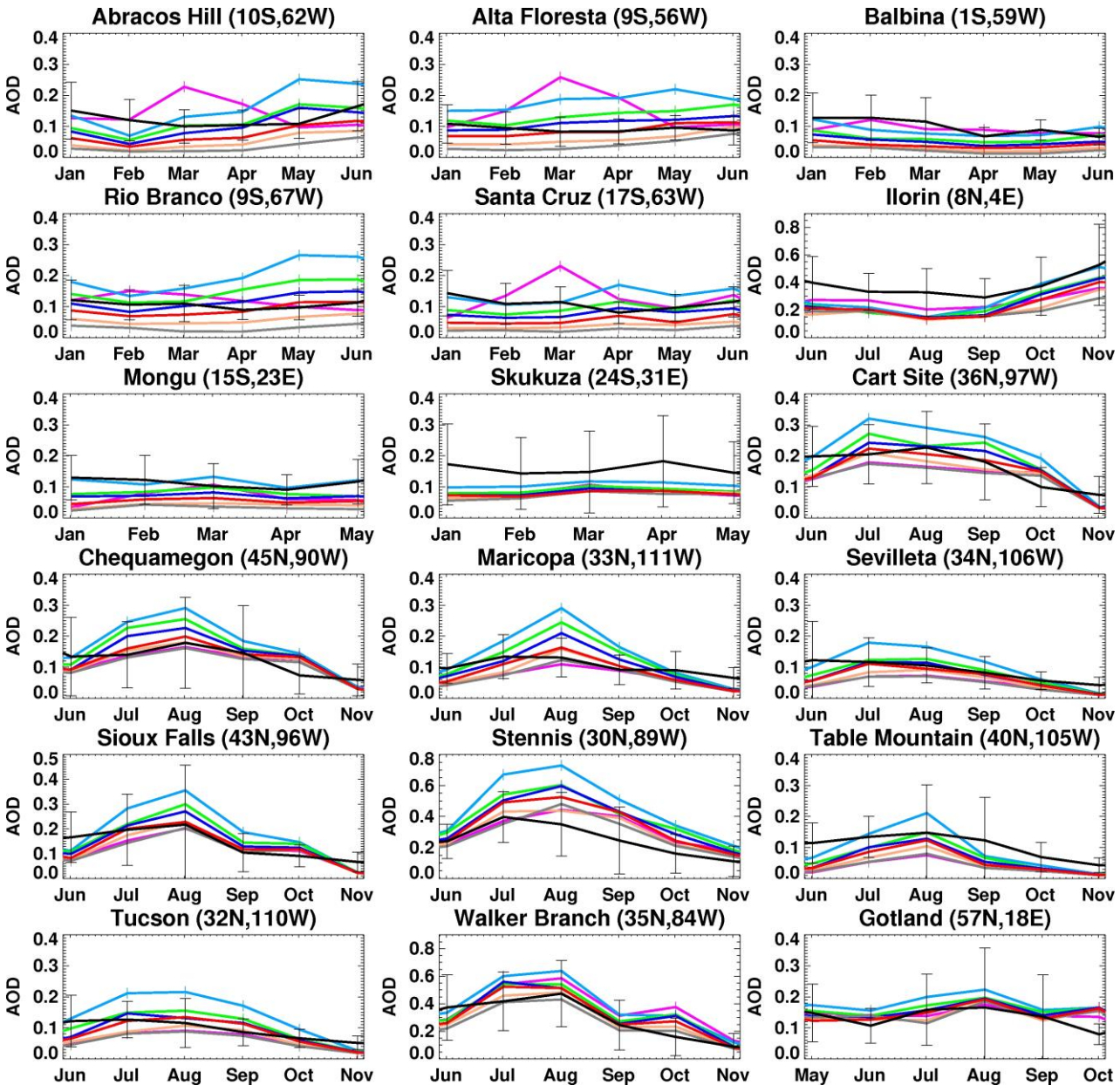

Supplementary Figure 1. Comparison of multi-year average observed AERONET (black lines) and simulated AOD at 18 different sites (see Methods), with error bars showing one standard deviation in multi-annual daily mean values. The colours correspond to the different simulations (see Methods): no SOA (grey), 17 Tg SOA a^{-1} (0.5×SOA, orange), 34 Tg SOA a^{-1} (1×SOA, red), 50 Tg SOA a^{-1} (1.5×SOA, blue), 67 Tg SOA a^{-1} (2×SOA, green), 100 Tg SOA a^{-1} (3×SOA, cyan) and GEOSChem (magenta).

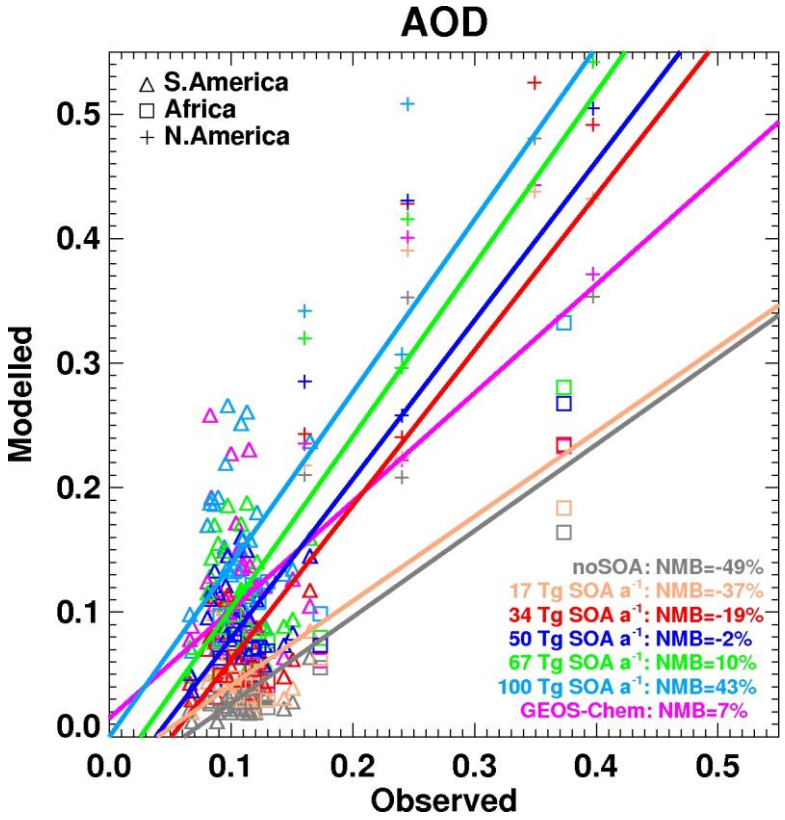

Supplementary Figure 2. Monthly-mean simulated AOD against corresponding observed values from 9 AERONET sites between 30°N-30°S (Abracos Hill, Alta Floresta, Balbina, Rio Branco, Santa Cruz, Ilorin, Mongu, Skukuza, Stennis) where biogenic SOA contributes more than 20% of total simulated monthly mean AOD. The AERONET AOD values shown are multi-annual monthly means calculated from all years of data available at each station. To minimise the effect of other aerosol (e.g. biomass burning), only values corresponding to January-June (South America, Mongu, Skukuza) and June-November (Ilorin, Stennis) were included. The colours correspond to the seven different simulations (see Methods): no SOA (grey), 17 Tg SOA a^{-1} (0.5×SOA, orange), 34 Tg SOA a^{-1} (1×SOA, red), 50 Tg SOA a^{-1} (1.5×SOA, blue), 67 Tg SOA a^{-1} (2×SOA, green), 100 Tg SOA a^{-1} (3×SOA, cyan) and GEOSChem (magenta). Lines of best fit (least absolute deviation method) between modelled and observed values for all sites and normalized mean biases (NMB) are included.

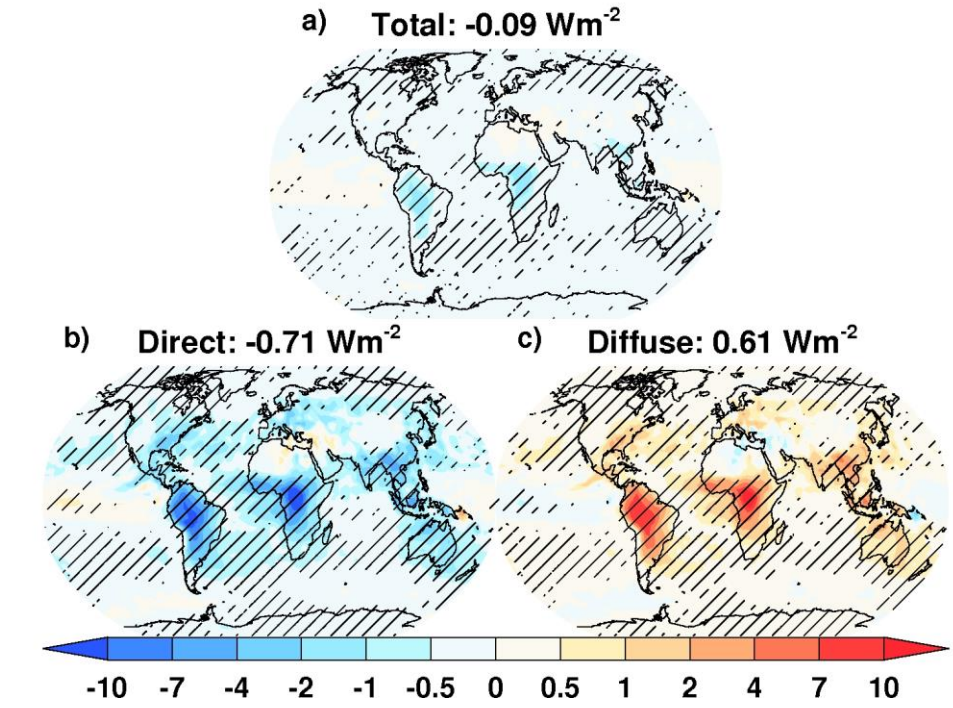

Supplementary Figure 3. Simulated annual mean changes in (a) total, (b) direct, and (c) diffuse solar radiation at the surface [W m^{-2}] caused by the biogenic SOA source simulated with GEOSChem. Values above panels are global averages. Hatches show areas where the changes are significant to the 95% confidence level.

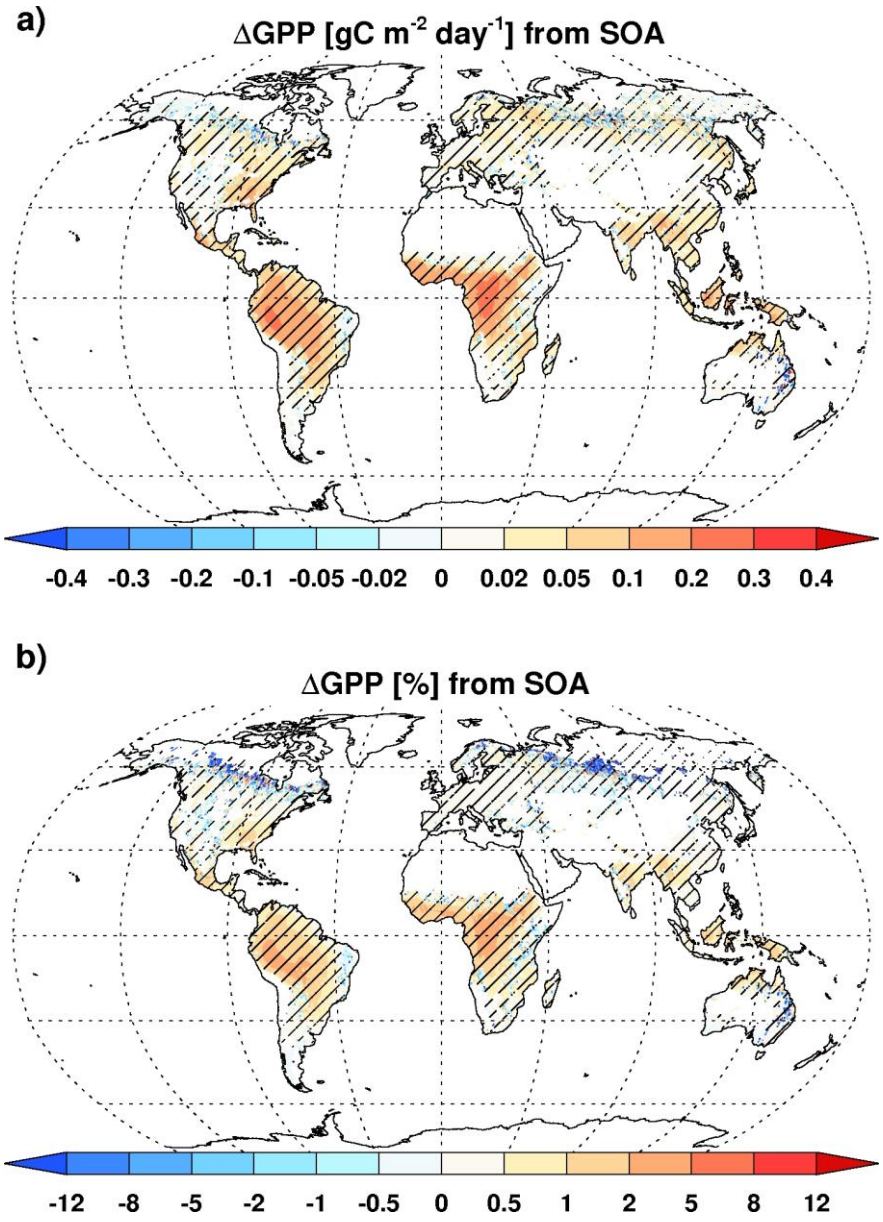

Supplementary Figure 4. Simulated distribution of annual mean (a) absolute [in gC m^{-2} day^{-1}] and (b) percentage [in %] changes in GPP from diffuse radiation fertilisation caused by the 50 Tg a^{-1} biogenic SOA emissions. Hatches show areas where the changes are significant to the 95% confidence level.

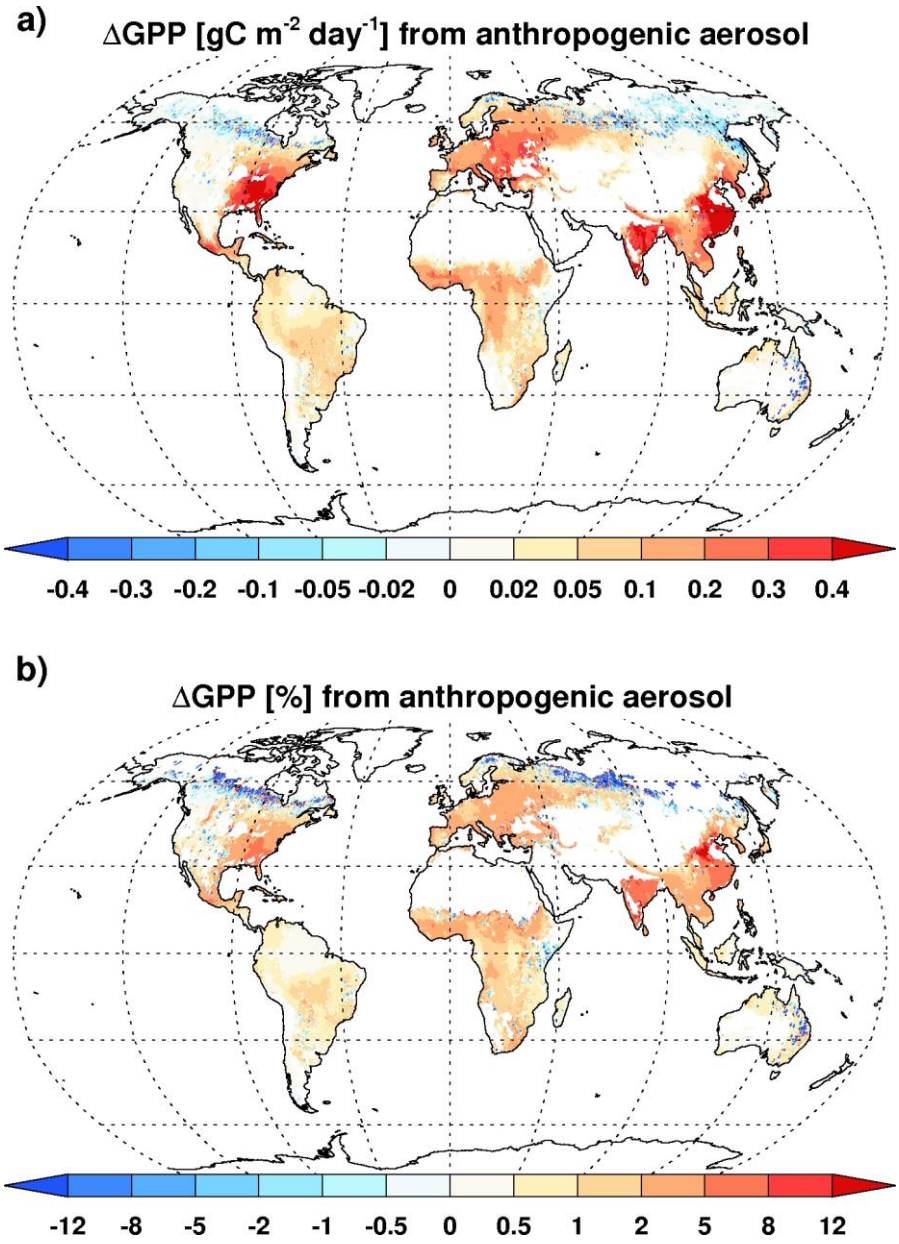

Supplementary Figure 5. Simulated distribution of annual mean (a) absolute [in gC m^{-2} day^{-1}] and (b) percentage [in %] changes in GPP from diffuse radiation fertilisation caused by present day anthropogenic aerosol emissions.

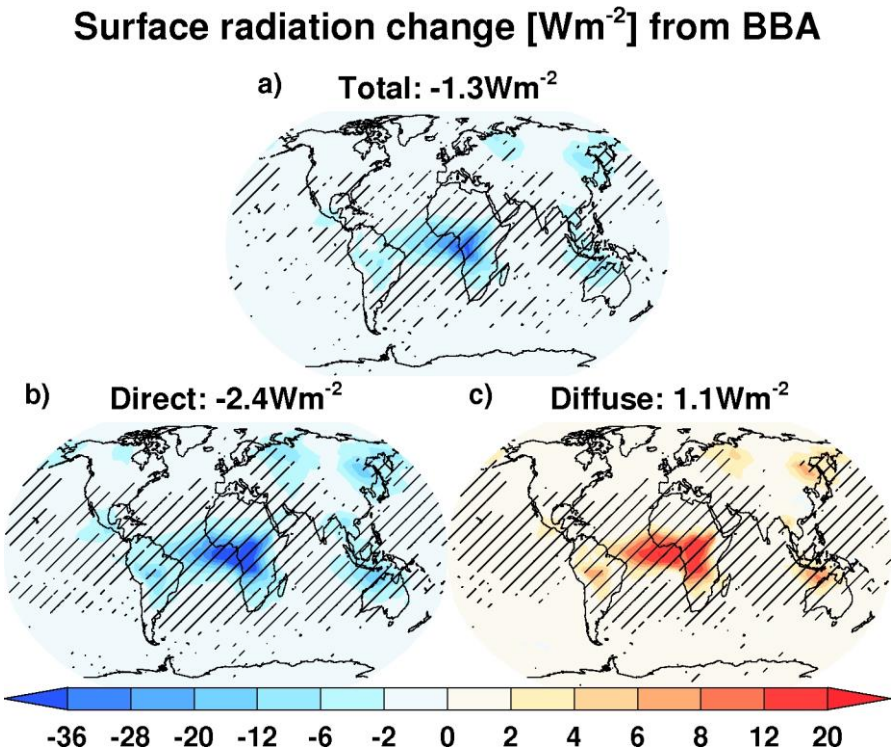

Supplementary Figure 6. Simulated annual mean changes in (a) total, (b) direct, and (c) diffuse solar radiation at the surface [W m^{-2}] caused by biomass burning aerosol (BBA). Values above panels are global averages. Hatches show areas where the changes are significant to the 95% confidence level.

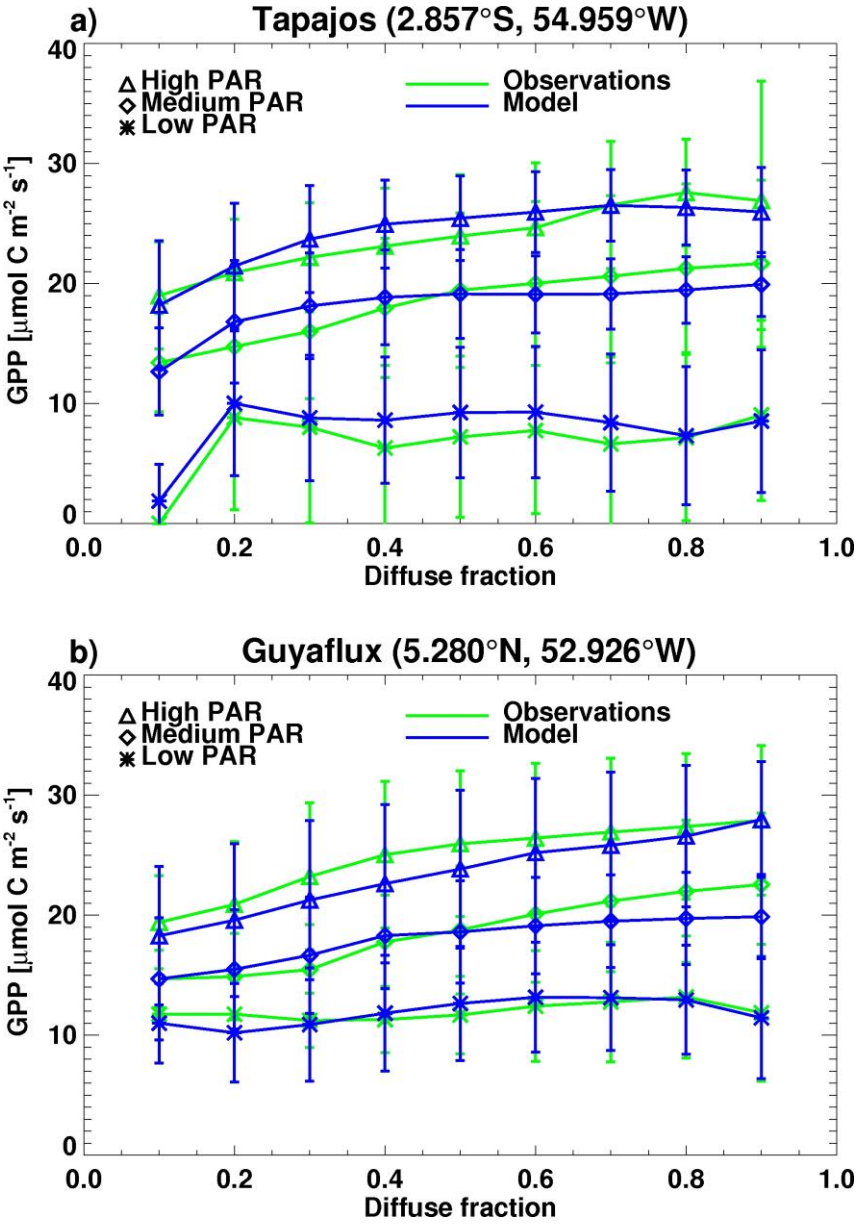

Supplementary Figure 7. Comparison of observed (green) and modelled (blue) GPP values as a function of diffuse radiation fraction at (a) Tapajos and (b) Guyaflux. Error bars show 1 standard deviation of all values. Data points are split into low (<500 μmol m^{-2} s^{-1}), medium (500<PAR<1000 μmol m^{-2} s^{-1}), and high (>1000 μmol m^{-2} s^{-1}) PAR conditions. The Guyaflux values correspond to 9 a.m.-5 p.m. local time only.

Supplementary Table 1. Simulated changes in global mean GPP and BVOC emissions due to the increase in diffuse radiation and the reduction in temperature resulting from a 10% increase in BVOC emissions.

	Diffuse radiation effect	Temperature effect
GPP	+0.08%	+0.01%
BVOC emission	+0.73%	-0.15%